

Spin-Peierls and Antiferromagnetic Phases in $\text{Cu}_{1-x}\text{Zn}_x\text{GeO}_3$: A Neutron Scattering Study

Michael C. Martin*, M. Hase†, K. Hirota‡, and G. Shirane

Department of Physics, Brookhaven National Laboratory, Upton, NY 11973-5000

Y. Sasago, N. Koide and K. Uchinokura

Department of Applied Physics, University of Tokyo, Bunkyo-ku, Tokyo 113, Japan

(March 30, 2018)

Abstract

Comprehensive neutron scattering studies were carried out on a series of high-quality single crystals of $\text{Cu}_{1-x}\text{Zn}_x\text{GeO}_3$. The Zn concentration, x , was determined for each sample using Electron Probe Micro-Analysis. The measured Zn concentrations were found to be 40-80% lower than the nominal values. Nevertheless the measured concentrations cover a wide range which enables a systematic study of the effects due to Zn-doping. We have confirmed the coexistence of spin-Peierls (SP) and antiferromagnetic (AF) orderings at low temperatures and the measured phase diagram is presented. Most surprisingly, long-range AF ordering occurs even in the lowest available Zn concentration, $x=0.42\%$, which places important constraints on theoretical models of the AF-SP coexistence. Magnetic excitations are also examined in

*Present address: Department of Physics, U.C. Berkeley, Berkeley, CA 94720-7300

†Present address: National Research Institute for Metals, 1-2-1 Sengen, Tsukuba, Ibaragi 305, Japan

‡Present address: Department of Physics, Tohoku University, Sendai 980-77, Japan

detail. The AF excitations are sharp at low energies and show no considerable broadening as x increases indicating that the AF ordering remains long ranged for x up to 4.7%. On the other hand, the SP phase exhibits increasing disorder as x increases, as shown from the broadening of the SP excitations as well as the dimer reflection peaks.

PACS: 75.25.+z, 75.30.Kz, 61.12.-q

I. INTRODUCTION

In 1993 the discovery of an inorganic spin-Peierls (SP) compound, CuGeO_3 , was first reported by Hase *et al.*¹ This material has chains of Cu^{2+} ($S = 1/2$) along its c -axis which distort into dimers below the SP transition temperature, $T_{SP} = 14.2\text{K}$.² The dimerized structure has a singlet ground state and a triplet excited state; singlet-to-triplet excitations were demonstrated by Nishi *et al.*³ using inelastic neutron scattering. CuGeO_3 is interesting not only because it is the first known inorganic spin-Peierls system, but also because evidence is mounting that it does not behave like a typical SP system. It has been believed that good one-dimensionality was needed for a material to undergo a spin-Peierls transition. However nearest-neighbor exchange parameters, estimated from the dispersions of magnetic excitations³ imply that the intrachain coupling is only 10 times stronger than the interchain coupling, which is far smaller than is found for other one-dimensional systems, typically 10^2 to 10^4 [7, 8]. Recent neutron-scattering measurements have revealed that the softening of a zone-boundary phonon as expected in ordinary SP systems does not exist.⁴ In addition, high-pressure neutron scattering studies^{5,6} have shown that as the pressure increases, T_{SP} and the SP energy gap increase while the lattice dimerization decreases, implying an additional mechanism, such as a spin-only effect, is at work. The susceptibility above T_{SP} ¹ and the critical exponent β of the SP energy gap^{9,10} both deviate substantially from the theoretical calculations of Bonner and Fisher¹¹ and Cross and Fisher¹² respectively, which work well for organic SP systems. Castilla *et al.*¹³ have recently proposed one possible theoretical model where the magnetic properties of CuGeO_3 can be well described by the one-dimensional Heisenberg model with competition between nearest-neighbor and next-nearest neighbor antiferromagnetic interactions.

Shortly after the discovery¹ of CuGeO_3 , a series of extensive studies were begun on samples with small amounts of dopant. Investigations have concentrated on systems where Cu atoms were replaced with Zn ¹⁴⁻¹⁹ or Ge was replaced with Si .²⁰⁻²² It is now well established that a new antiferromagnetic (AF) ordered phase appears at low temperatures in

both Zn-doped^{14,19} and Si-doped²² samples. A preliminary phase diagram was determined from susceptibility measurements on powder samples¹⁴ which showed that T_{SP} decreases with increasing Zn concentration while the Néel temperature increases to $T_N \sim 4\text{K}$. This phase diagram was recently confirmed using single crystals^{15,19} and in Figure 1 we present the phase diagram as determined from neutron and susceptibility measurements on all single crystals produced for the present study. The most intriguing feature reported so far in these doped CuGeO_3 systems is the coexistence of the SP and AF states below the Néel temperature. This was first demonstrated by Regnault *et al.*²² who used neutron scattering to observe the SP order parameter, i.e. the lattice dimerization, become smaller but still finite below T_N . Sasago *et al.*¹⁹ showed that the SP and AF states also coexist for samples having a nominal range of 2 – 6% Zn. The coexistence of a SP singlet state and AF ordering was quite a surprise since it was thought that these two ordered states were mutually exclusive, and it adds another puzzle to the already unusual SP state in CuGeO_3 . Recently, Fukuyama *et al.*²³ have proposed a theoretical model for disorder-induced antiferromagnetic long range order within a spin-Peierls system. This model concludes that an infinitesimal amount of impurity can induce a long-range AF state in a spin-gap system (which includes spin-ladders and two dimensional systems, as well as SP systems). The comparison of this theory with our experimental results will be presented.

In the present paper comprehensive neutron scattering results are presented studying Zn-doped CuGeO_3 single crystals grown by the floating-zone (FZ) method. The amount of Zn-dopant, x , was carefully determined using Electron Probe Micro-Analysis (EPMA) for each crystal. The SP dimerization and the AF magnetic moment are surveyed as a function of x . Magnetic excitations in both the SP and the SP-AF coexistence states were studied in detail as a function of temperature, q , and x yielding some important conclusions about the interplay of the AF and SP states.

II. EXPERIMENTAL DETAILS

A. Sample Preparation

A series of relatively large ($\sim 0.4 \text{ cm}^3$) $\text{Cu}_{1-x}\text{Zn}_x\text{GeO}_3$ single crystals having *nominal* Zn concentrations of 1, 2, 4, 6, and 8% were grown using the floating-zone (FZ) method. The crystals grow along the c -axis (the chain direction) and typically had mosaic spreads of less than 0.3 degrees. As shown in Figure 2, the crystals were cut into several parts for characterization using Electron Probe Micro-Analysis (EPMA) and measurements of neutron scattering and susceptibility. Typical susceptibilities along the c direction for several values of x are shown in the lower part of Figure 2. The EPMA analysis revealed that the true Zn concentrations were consistently lower than the nominal values: the average measured values of x are 0.42, 0.9, 3.2, 2.1, and 4.7% corresponding to the nominal values of 1, 2, 4, 6, and 8%, respectively.

As the Zn concentration increases, it becomes more difficult to grow a single crystal with a single domain. In order to obtain high quality single crystals with small mosaic spreads, the speed at which the zone is moved must be kept slow. On the other hand, impurities (Zn atoms) tend to be purged from the melted zone if the growth process is too slow. It is thus difficult to fabricate crystals both of high quality and with high Zn concentration. We were able to grow crystals with a fairly wide range of Zn concentrations enabling a systematic study of the effects of Zn doping. The homogeneity of the Zn concentrations was checked by measuring various regions ($2 \times 2 \mu\text{m}^2$ each) of the samples by EPMA. These homogeneities are quoted as uncertainties in Table I which also presents the crystal volumes and measured transition temperatures. Both SP and AF transitions are quite sharp, consistent with small error bars in the actual Zn concentrations.

B. Neutron Scattering Spectrometers

Neutron scattering measurements were carried out using triple-axis spectrometers on the H7 and H8 (14.7 meV incident energy neutrons), and H9a (5 meV) beamlines of the

High Flux Beam Reactor at Brookhaven National Laboratory. The crystals were mounted in helium filled aluminum cans which were subsequently attached to the cold finger of a cryostat. The samples were aligned so as to place the $(0\ k\ l)$ or $(h\ k\ h)$ zones in the experimental scattering plane. Incident neutrons with energies of 14.7 or 5.0 meV were selected by a pyrolytic graphite (PG) $(0\ 0\ 2)$ monochromator; PG $(0\ 0\ 2)$ was also used for an analyzer. To eliminate higher-order harmonics, PG filters were placed before the sample and after the analyzer. The beam was horizontally collimated, typically $40'$ - $40'$ -Sample- $40'$ - $80'$ in sequence from the reactor core to the detector. Tighter collimations were used for some of the higher resolution measurements presented. When comparing the intensities of dimerization and magnetic superlattice peaks between the various crystals, Bragg peaks unaffected by extinction are required for use as normalization. The weak $(0\ 2\ 1)$ and $(1\ 2\ 1)$ peaks fill this need and are used for our data analysis.

III. ORDER PARAMETERS

A. Phase Diagram

The transition temperatures T_{SP} and T_N , where the sample enters the SP and AF states respectively, were determined for each crystal using both magnetic susceptibility measurements and observing critical scattering peaks in the neutron studies. Figure 3 plots the intensity of the SP and AF superlattice peaks as a function of temperature for 3.2 and 0.42% Zn-doped samples. T_{SP} and T_N for each crystal are summarized in Table I. The full phase diagram including susceptibility data from numerous crystals is presented in Figure 1.

The most significant result here is that AF ordering is observed for even the smallest available amounts of Zn, $x = 0.42\%$. As shown in Figure 3(b), the AF superlattice peak is nearly resolution limited demonstrating that a long-ranged Néel ordering is induced by very small amounts of Zn impurities. A second interesting result is that T_{SP} and T_N change as

x is increased to about 2%, but then do not change much for Zn concentrations exceeding 2%.

B. Dimerization

Hirota *et al.*² determined that as the dimerization occurs below T_{SP} , the $(\frac{h}{2} \ k \ \frac{l}{2})$ superlattice peaks, with h and l odd and k any integer, appear. The intensities of the SP superlattice peaks decrease continuously as a function of increasing Zn content indicating a weakening SP dimerization. The transition is less sharp in the Zn-doped crystals compared to pure CuGeO_3 , and it can be estimated by fitting the data with a power law model which includes a Gaussian distribution of transition temperatures.

Using the maximum intensity of these SP superlattice peaks (at about 6 K), the dimerizing atomic displacement, δ , can be calculated as compared to the displacement in pure CuGeO_3 , which we define as δ_0 . To normalize with respect to crystal volume, the extinction-free $(1 \ 2 \ 1)$ Bragg peak is used as a reference for each sample. The structural factor F is calculated for each peak using the relation $F = \sqrt{I \sin 2\theta}$, where I is the measured intensity and θ is the scattering angle. The approximate atomic displacements are now calculated for each dopant level by comparing the ratio $F_{\text{obs}}(\frac{1}{2} \ 3 \ \frac{1}{2})/F_{\text{obs}}(1 \ 2 \ 1)$ for each Zn-doped sample to the known ratio in the undoped case. The numerical results are presented in Table I. As the Zn-doping increases, the average atomic distortion is reduced dramatically; by adding only 1% Zn the dimerizing atomic shift loses 1/3 of its magnitude.

C. Antiferromagnetic moment

Hase *et al.*¹⁴ found that the AF ordering is associated with a superlattice reflection at $(0 \ 1 \ \frac{1}{2})$. The magnetic moment of the AF state can be calculated from the observed intensity of this peak. Using the $(0 \ 2 \ 1)$ peak as an extinction-free normalization, we compare the $F_{\text{obs}}(0 \ 1 \ \frac{1}{2})/F_{\text{obs}}(0 \ 2 \ 1)$ ratio to the ratio previously measured by Hase *et al.*¹⁸ for a different 3.4% Zn-doped crystal. Hase *et al.* calculated the magnetic moment, μ_{eff} , extrapolated

to zero temperature for that sample to be $\mu_{eff} = 0.22\mu_B$. By comparing the normalized superlattice peak intensities, values for the magnetic moments of each of the Zn-doped samples are obtained, and are summarized in Table I. In all Zn-doped samples studied the SP dimer superlattice peak loses some intensity below T_N . Since the superlattice peak intensity is directly related to the atomic displacements ($I \propto \delta^2$) this observation shows that the dimers are indeed adversely affected by the onset of a Néel ordering.

Figure 4 shows the SP atomic dimerization δ at 6 K and the AF magnetic moment μ_{eff} at 0 K as a function of Zn concentration x . μ_{eff} is found to scale with T_N very well, showing a linear relation, as demonstrated in the bottom panel of Figure 4. As mentioned previously, the resolution-limited peak width shown in Fig. 3(b) indicates a long-range AF ordering; this is true for all samples. However, the SP reflections exhibit line broadening for 3.4 and 4.7% Zn-doped samples.

IV. MAGNETIC EXCITATIONS

A. Spin-Peierls Excitations

In the SP state of CuGeO_3 excitations were observed to have an energy gap of 2.1 meV at $q = (0, 1, 0.5)$ [3]. Hase *et al.*¹⁸ reported that the magnetic excitations in a 3.4% Zn-doped CuGeO_3 crystal are overdamped. Magnetic excitations in Si-doped CuGeO_3 have also been recently reported by Regnault *et al.*²² where, in contrast to Hase *et al.*, the excitations remain well defined (are underdamped). Extensive measurements of the magnetic excitation spectra were obtained in all of the Zn-doped crystals of the present study. Some preliminary results were presented by Sasago *et al.*¹⁹ In the subsequent examination of all other compositions, well-defined (underdamped) magnetic excitations were found. Therefore the 3.4% Zn-doped crystal used by Hase *et al.*¹⁸ is the only sample in which overdamped excitations were observed.

The measurements were extended to a wider range of q within the $(0 k l)$ zone to deter-

mine the dispersion along b^* and c^* . A summary of the measured dispersions is presented in Fig. 5. As in pure CuGeO_3 , the dispersion is much steeper in the c^* direction compared to b^* . A small decrease in the SP energy gap magnitude is observed throughout the zone upon increasing Zn concentration. However the excitations remain well defined and are only somewhat broadened. This broadening is demonstrated in Fig. 6, where an excitation profile at $q = (0, 1.1, 0.5)$ for 3.2% Zn is compared with those of pure and 0.9% Zn samples. By convolving the proper resolution function with a dispersion surface, the intrinsic line widths Γ are extracted for 0, 0.9% and 3.2% Zn to be $\Gamma = 0.22, 0.31, \text{ and } 1.09$ meV, respectively. The solid lines in the figure are the resultant fits.

To try to clear up the discrepancy between the present results and those of Hase *et al.*¹⁸, the 3.4% Zn sample used in that earlier study was re-examined. This sample was found to have a reasonably well defined peak only at higher energy transfer. Thus the overdamped modes observed in the Hase sample are limited to low energy SP magnetic excitations. We speculate that the AF modes may be underdamped in Hase's 3.4% Zn sample.

B. AF Excitations

Regnault and co-workers²² reported finding sharp AF magnetic excitations at energies of 0.2 meV at the magnetic zone center in their 0.7% Si doped sample. Using electron spin resonance (ESR) Hase *et al.*²⁴ recently observed an antiferromagnetic resonance below $T_N = 4.2\text{K}$ in a $\text{Cu}_{0.96}\text{Zn}_{0.04}\text{GeO}_3$ crystal, which indicates spin-wave excitations (AF modes) at the magnetic-zone center at energies of 0.11 and 0.17 meV.²⁴ We therefore searched for these AF excitation modes in our neutron studies of our best characterized higher doped crystal which has 3.4% Zn.

In our search for AF excitations, we encountered considerable difficulties mostly due to various kinds of spurious peaks appearing through the resolution function. After experimenting with two incident neutron energies and three different scattering zones, the proper experimental window was found in which the AF excitations can be characterized in a wide

enough q - E range. Figure 7 depicts how the AF mode is sharp at low q values, but becomes significantly broadened at larger values of b^* . Figure 8 demonstrates the dispersion and broadening which occurs as a function of q along a^* . The AF mode along c^* appears to be broad even for small q . It seems that the broadening occurs when the transfer energy, rather than q , exceeds a certain value. It is interesting to note that the broadening at higher q values is exactly opposite to the SP modes which are sharp at high q and broaden dramatically at smaller q . The AF excitation data are combined into full dispersion relations which are presented in Figure 9, along with q maps showing where the measurements were carried out.

V. DISCUSSION

As we have already emphasized, the AF ordering in the $\text{Cu}_{1-x}\text{Zn}_x\text{GeO}_3$ system takes place for as little as 0.42% Zn which has a $T_N = 0.6$ K. It is now established that a very small Zn concentration is sufficient for long range AF ordering and that this long-range AF order is present in all Zn concentrations studied. These remarkable results have immediate consequences on theoretical models. Percolation type descriptions are ruled out as they would predict the onset of AF only after a certain amount of impurity islands have been formed; when the amount of Zn is too small, long range order could not exist in such a system. The present results instead lend weight to a theoretical model recently proposed by Fukuyama *et al.*²³ which predicts a standing wave long range order for arbitrarily small amounts of an impurity within a SP system, probably even at $x = 0$ for perfect crystals. Our data of AF ordering in a 0.42% Zn crystal strongly support this theoretical prediction.

In contrast to the long-range correlations in the AF state, the SP phase exhibits increasing disorder with increasing Zn concentration; the SP superlattice reflection at (1.5, 1, 1.5) shows considerable line broadening with increasing x . Two recent x-ray studies^{25,26} generally agree with our results, one measures the line widths, and the other takes a new approach using critical scattering. It will be interesting to learn how the SP phase is grad-

ually destroyed at high x values. It may be in this aspect where the distinction between site substitution of Zn for Cu is different from the bond disorder in substitution of Si for Ge. The ability to grow uniform, large x single crystals of $\text{Cu}_{1-x}\text{Zn}_x\text{GeO}_3$ is necessary for further quantitative studies. As discussed in the sample preparation description above, this ability is still forthcoming.

In the present study, evidence for AF and SP orderings have been presented along with detailed quantitative results for AF magnetic moment μ_{eff} and dimerization δ as a function of Zn concentration x . One important finding is that μ_{eff} scales well with T_N . In addition, key characteristics of SP and AF magnetic excitations have been established. Contrasting behaviors are found in these excitations. The AF excitations show a distinctive peak in the small q and energy region. As the energy transfer increases, the AF excitation rapidly broadens, and above 1 meV it becomes indistinguishable from the background. On the other hand, the SP excitations show considerable line-broadening as the Zn concentration is increased, and this peak broadens at smaller q as well. These results will serve as critical tests for forthcoming theoretical models of this fascinating compound.

So far the problem has been treated as if the Zn content x is the only parameter with which to characterize the $\text{Cu}_{1-x}\text{Zn}_x\text{GeO}_3$ system. There may be other issues at play, such as exact oxygen stoichiometry (which can have dramatic effects in other well-known oxide systems). Closer inspection of Table I reveals immediately that T_N , μ_{eff} , and δ are not smooth functions of x . It may, in part, be due to inaccuracies in the experiments, but the variation is too large to be completely assigned to experimental errors. And the fact that the Hase 3.4% sample does not quite fit into the overall scheme remains a puzzle. Another example of how much is still to be learned about the CuGeO_3 system is the variance of T_{SP} even for $x = 0$. An undoped crystal which is our most perfect crystallographically has a T_{SP} of 13.2 K, one full degree lower than the accepted value of 14.2 K.

After writing this paper we became aware of a manuscript by Coad *et al.*²⁷ which discusses elastic neutron measurements of CuGeO_3 where Cu has been replaced by Zn or Ni. They similarly report a degradation of the SP state with the onset of AF ordering and their

resultant phase diagram is close, although not identical, to the one reported here. Overall their work and the present results lend support to each other.

ACKNOWLEDGMENTS

We would like to thank R.J. Birgeneau, Guillermo Castilla, and Vic Emery for stimulating discussions. Thanks to S. Coad, H. Fukuyama, and L.P. Regnault for providing their manuscripts prior to publication and for informative private discussions. We also are pleased to acknowledge the expert technical help of J. Biancarosa, N. Donahue, B. Liegel, K. Mohanty, and R. Rothe of the BNL HFBR Physics staff. This work was supported in part by the U.S.- Japan Cooperative Research Program on Neutron Scattering, and a NEDO (New Energy and Industrial Technology Development Organization) International Joint Research Grant. Research at Brookhaven National Laboratory was supported by the Division of Materials Research at the U.S. Department of Energy, under contract No. DE-AC02-76CH00016.

REFERENCES

- ¹ M. Hase, I. Terasaki, and K. Uchinokura, Phys. Rev. Lett. **70**, 3651 (1993).
- ² K. Hirota, D.E. Cox, J.E. Lorenzo, G. Shirane, J.M. Tranquada, M. Hase, K. Uchinokura, H. Kojima, Y. Shibuya, and I. Tanaka, Phys. Rev. Lett. **73**, 736 (1994).
- ³ M. Nishi, O. Fujita, and J. Akimitsu, Phys. Rev. B **50**, 6508 (1994).
- ⁴ K. Hirota, G. Shirane, Q. J. Harris, Q. Feng, R. J. Birgeneau, M. Hase, and K. Uchinokura, Phys. Rev. B **52**, 15412 (1995).
- ⁵ S. Katano, O. Fujita, J. Akimitsu and M. Nishi, Phys. Rev. B **52**, 15364 (1995).
- ⁶ M. Nishi, O. Fujita, J. Akimitsu, K. Kakurai, and Y. Fujii, Phys. Rev. B **52**, R6959 (1995).
- ⁷ W.J.L. Buyers *et al.*, Phys. Rev. Lett. **56**, 371 (1986).
- ⁸ J.P. Renard *et al.*, Europhys. Lett. **3**, 945 (1987).
- ⁹ Michael C. Martin, G. Shirane, Y. Fujii, M. Nishi, O. Fujita, J. Akimitsu, M. Hase, and K. Uchinokura, Phys. Rev. B **53**, R14713 (1996).
- ¹⁰ J.-G. Lussier, S.M. Coad, D.F. McMorrow, and D. McK. Paul, J. Phys. Condens. Matter **8**, L59 (1996).
- ¹¹ J.C. Bonner and M.E. Fisher, Phys. Rev. **135**, A640 (1964).
- ¹² M.C. Cross and D.S. Fisher, Phys. Rev. B **19**, 402 (1979); M.C. Cross, Phys. Rev. B **20**, 4606 (1979).
- ¹³ G. Castilla, S. Chakravarty, and V. J. Emery, Phys. Rev. Lett. **75**, 1823 (1995).
- ¹⁴ M. Hase, I. Terasaki, Y. Sasago, K. Uchinokura and H. Obara, Phys. Rev. Lett. **71**, 4059 (1993).
- ¹⁵ M. Hase, N. Koide, K. Manabe, Y. Sasago, K. Uchinokura, and A. Sawa, Physica B **215**, 164 (1995).

- ¹⁶ S.B. Oseroff, S.-W. Cheong, B. Aktas, M.F. Hundley, Z. Fisk, and L.W. Rupp, Jr., *Phys. Rev. Lett.* **30**, 74 (1995).
- ¹⁷ J.G. Lussier, S.M. Coad, D.F. McMorrow and D. McK. Paul, *J. Phys. Condens. Matter* **7**, L325 (1995).
- ¹⁸ M. Hase, K. Uchinokura, R.J. Birgeneau, K. Hirota and G. Shirane, *J. Phys. Soc. Japan* **65**, 1392 (1996).
- ¹⁹ Y. Sasago, N. Koide, K. Uchinokura, Michael C. Martin, M. Hase, K. Hirota, and G. Shirane, *Phys. Rev. B* **54**, R6835 (1996).
- ²⁰ J.P. Renard, K. LeDang, P. Veillet, G. Dhalenne, A. Revcolevschi, and L.P. Regnault, *Europhys. Lett.* **30**, 475 (1995).
- ²¹ M. Poirier, R. Beaudry, M. Castonguay, M.L. Plumer, G. Quirion, F.S. Razavi, A. Revcolevschi and G. Dhalenne, *Phys. Rev. B* **52**, R6971 (1995).
- ²² L.P. Regnault, J.P. Renard, G. Dhalenne, and A. Revcolevschi, *Europhys. Lett.* **32**, 579 (1995).
- ²³ H. Fukuyama, T. Tanimoto, and M. Saito, *J. Phys. Soc. Japan* **65**, 1182 (1996).
- ²⁴ M. Hase, M. Hagiwara, and K. Katsumata, *Phys. Rev. B* **54**, R3722 (1996).
- ²⁵ J. P. Schoeffel, J. P. Pouget, G. Dhalenne, and A. Revcolevschi, *Phys. Rev. B* **53**, 14971 (1996).
- ²⁶ V. Kiryukhin, B. Keimer, J. P. Hill, S. M. Coad, and D. McK. Paul, *Phys. Rev. B* **54**, 7269 (1996).
- ²⁷ S. Coad, J.-G. Lussier, D.F. McMorrow, and D. McK. Paul, *J. Phys. Condens. Matter* **8**, 6251 (1996).

TABLES

TABLE I. Numerical values for the SP and AF transition temperatures, and the atomic shifts and magnetic moments for the SP and AF states, respectively, for all $\text{Cu}_{1-x}\text{Zn}_x\text{GeO}_3$ crystals studied.

Identification	Zn	Crystal Volume (cm^3)	SP		AF	
	x (%)		T_{SP} (K)	$\delta(6\text{K})$	T_N (K)	$\mu_{eff}(0\text{K})$
N 1	0.42 ± 0.14	0.03	13.6	0.72	0.6	0.06
–	0.74	0.01	12.5	0.60	2.4	0.14
N 2	0.91 ± 0.20	0.4	12.5		2.0	0.10
N 6	2.1 ± 0.3	0.4	10.2	0.26	4.2	0.24
N 4	3.2 ± 0.4	0.4	10.3	0.40	4.1	0.18
Hase 4	3.4	0.04	10.0		4.2	0.22
N 8	4.7	0.1	10.0		4.3	0.19

FIGURES

FIG. 1. Newly established magnetic phase diagram of $\text{Cu}_{1-x}\text{Zn}_x\text{GeO}_3$ by the present neutron-scattering studies (open circles) in combination with magnetic susceptibility measurements (filled circles).

FIG. 2. Sketches of some of the flux-grown crystals used in the present study. The sections of each crystal are labeled as to what experiments were carried out on them: SUS (susceptibility), EPMA (Electron Probe Micro-Analysis), and Neutron scattering. Examples of the temperature dependence of the measured susceptibility along the c -direction is presented in the lower part of the figure for pure, 0.91% and 3.2% Zn-doped crystals.

FIG. 3. (a) Intensities of SP and AF superlattice peaks as a function of temperature for a 3.2% Zn-doped crystal. The two transition temperatures are clearly observable and are indicated on in the plot. (b) Temperature dependence of an AF superlattice peak for a 0.42% Zn-doped crystal. The inset shows a peak profile of the AF superlattice peak, indicating that the width is resolution limited.

FIG. 4. (a) Dimerization (δ) at 6 K as a function of Zn concentration (x). (b) AF magnetic moment (μ_{eff}) extrapolated to 0 K as a function of x . (c) μ_{eff} correlates linearly with T_N .

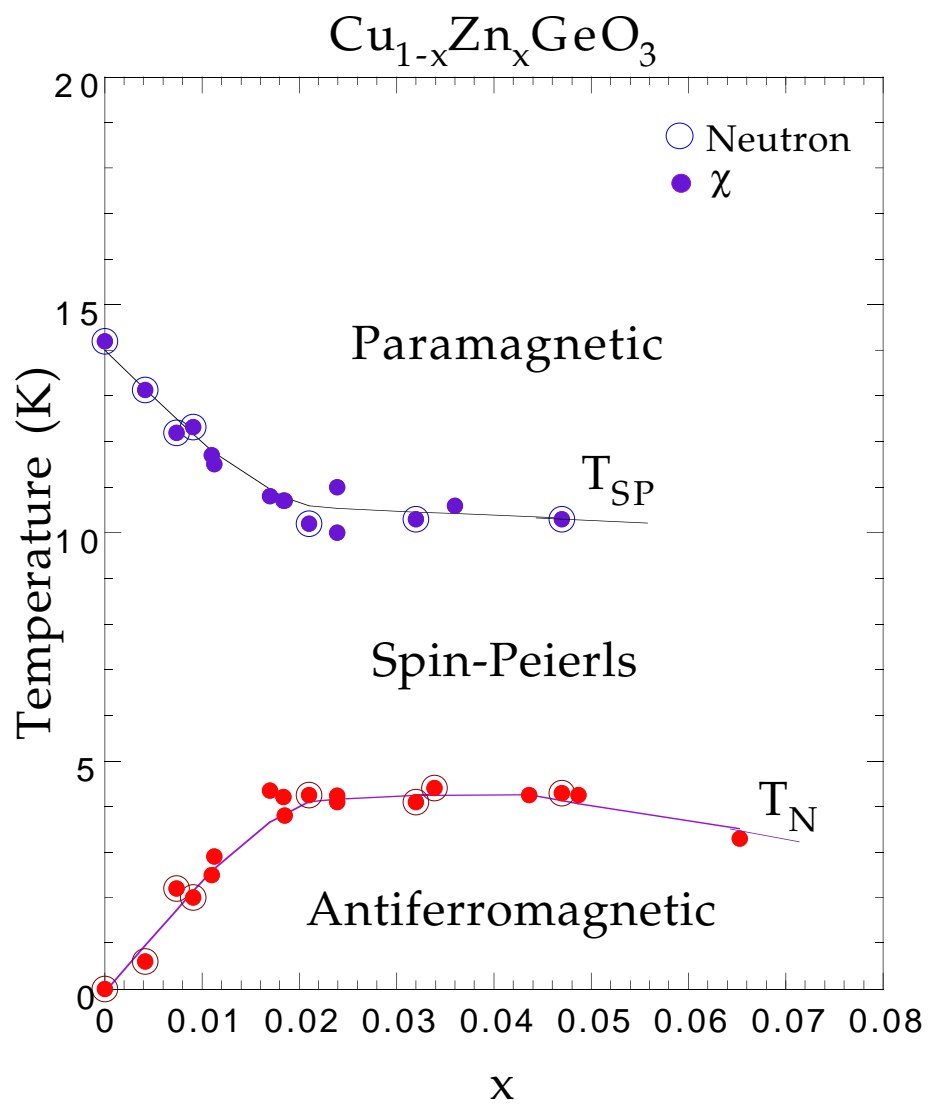
FIG. 5. The measured dispersions of the SP magnetic excitation in the b^* and c^* directions. The different symbols represent different Zn concentrations as denoted in the legend.

FIG. 6. SP excitations of $\text{Cu}_{1-x}\text{Zn}_x\text{GeO}_3$ for $x = 0, 0.009, 0.032$ above T_N of each sample. Data are fitted with a scattering function described in the text with a proper resolution correction, in order to extract an intrinsic energy width Γ of the excitation.

FIG. 7. SP as well as AF excitations for a 3.2% Zn-doped sample measured at $E_i = 5.0$ meV. The AF mode can be seen clearly, its energy width is resolution limited at small q , but becomes significantly broadened at higher q . Lines are guides to the eye.

FIG. 8. Energy spectra of AF excitations for a 3.2% Zn-doped sample measured at q positions along the a^* direction, which has considerably less dispersion than in the b^* or c^* directions.

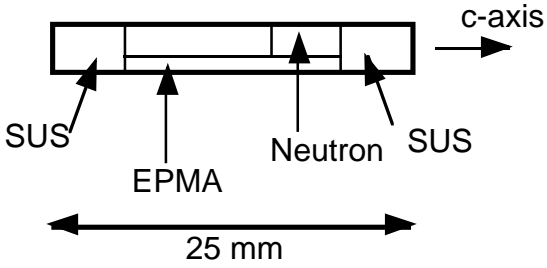
FIG. 9. The measured dispersions of the SP as well as AF magnetic excitations in the b^* , c^* and a^* directions. Insets shows where in q -space the scans were obtained.



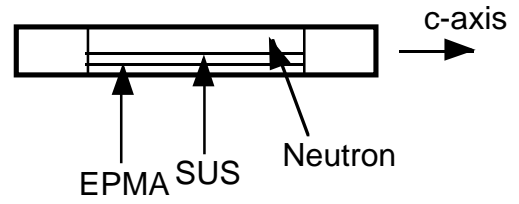
Martin et al., Fig. 1

Cu_{1-x}Zn_xGeO₃ Sample Preparation

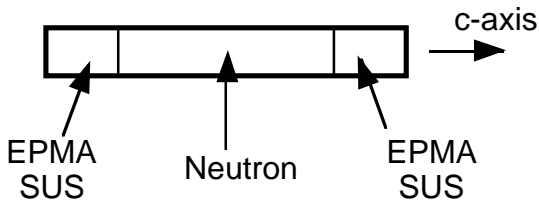
Nominal Zn Concentration: 1%
Analyzed Zn Concentration: 0.42%



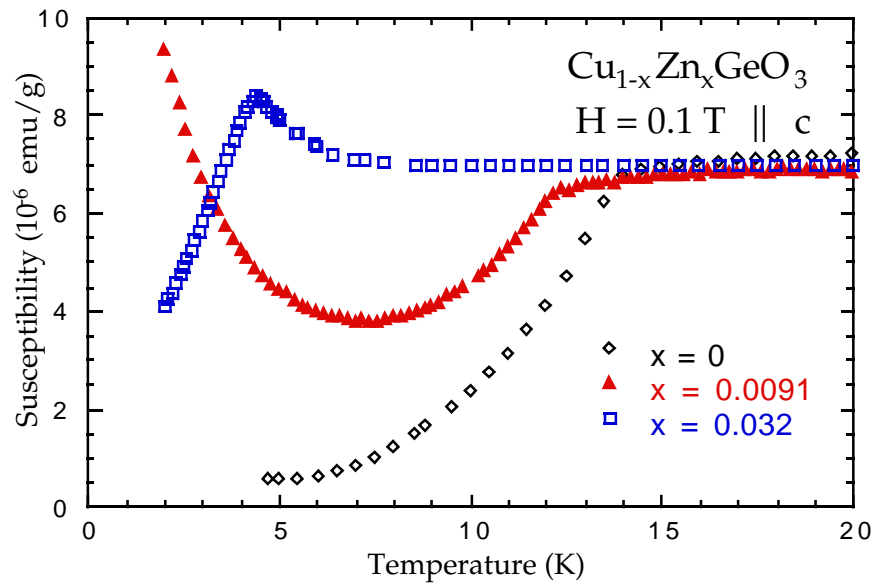
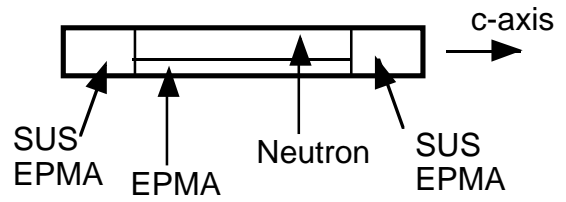
Nominal Zn Concentration: 2%
Analyzed Zn Concentration: 0.91%

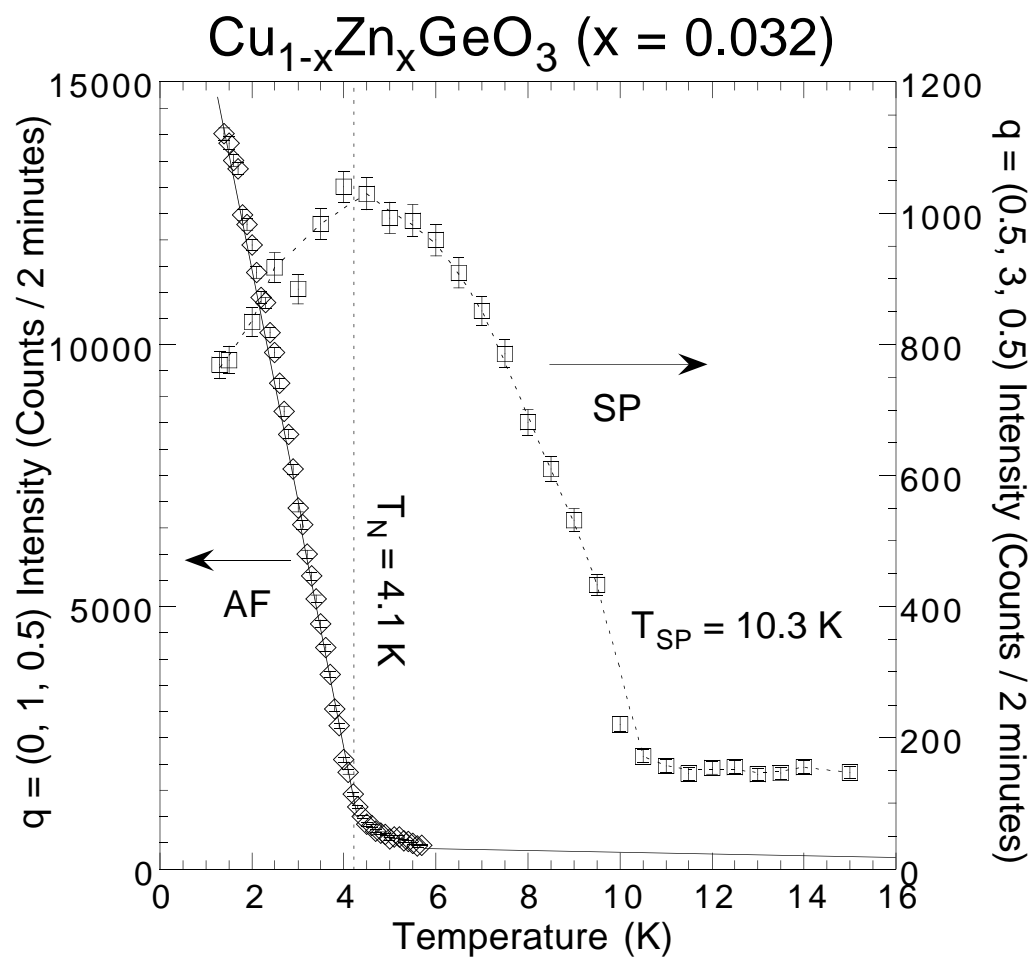


Nominal Zn Concentration: 4%
Analyzed Zn Concentration: 3.2%

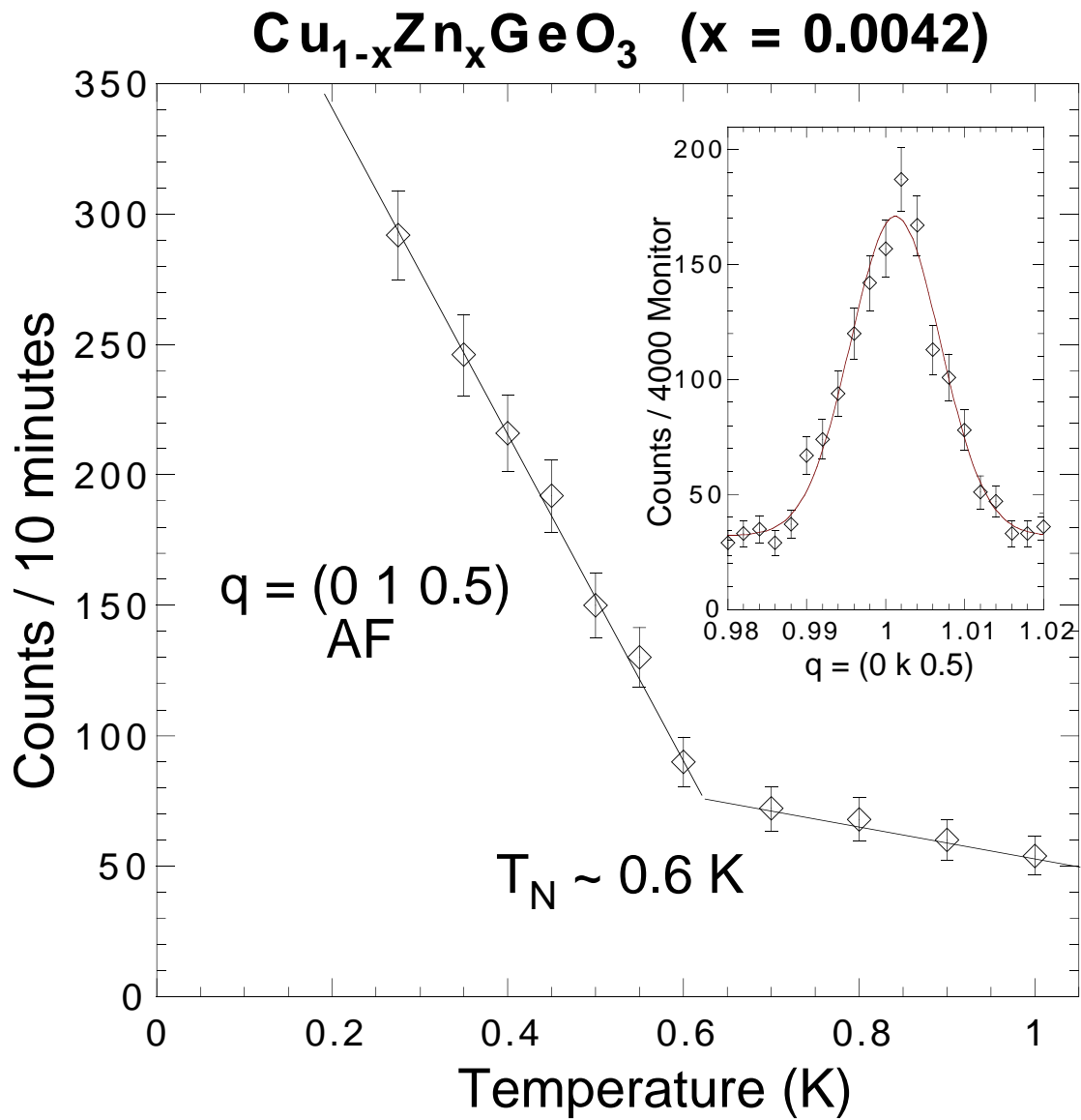


Nominal Zn Concentration: 6%
Analyzed Zn Concentration: 2.1%

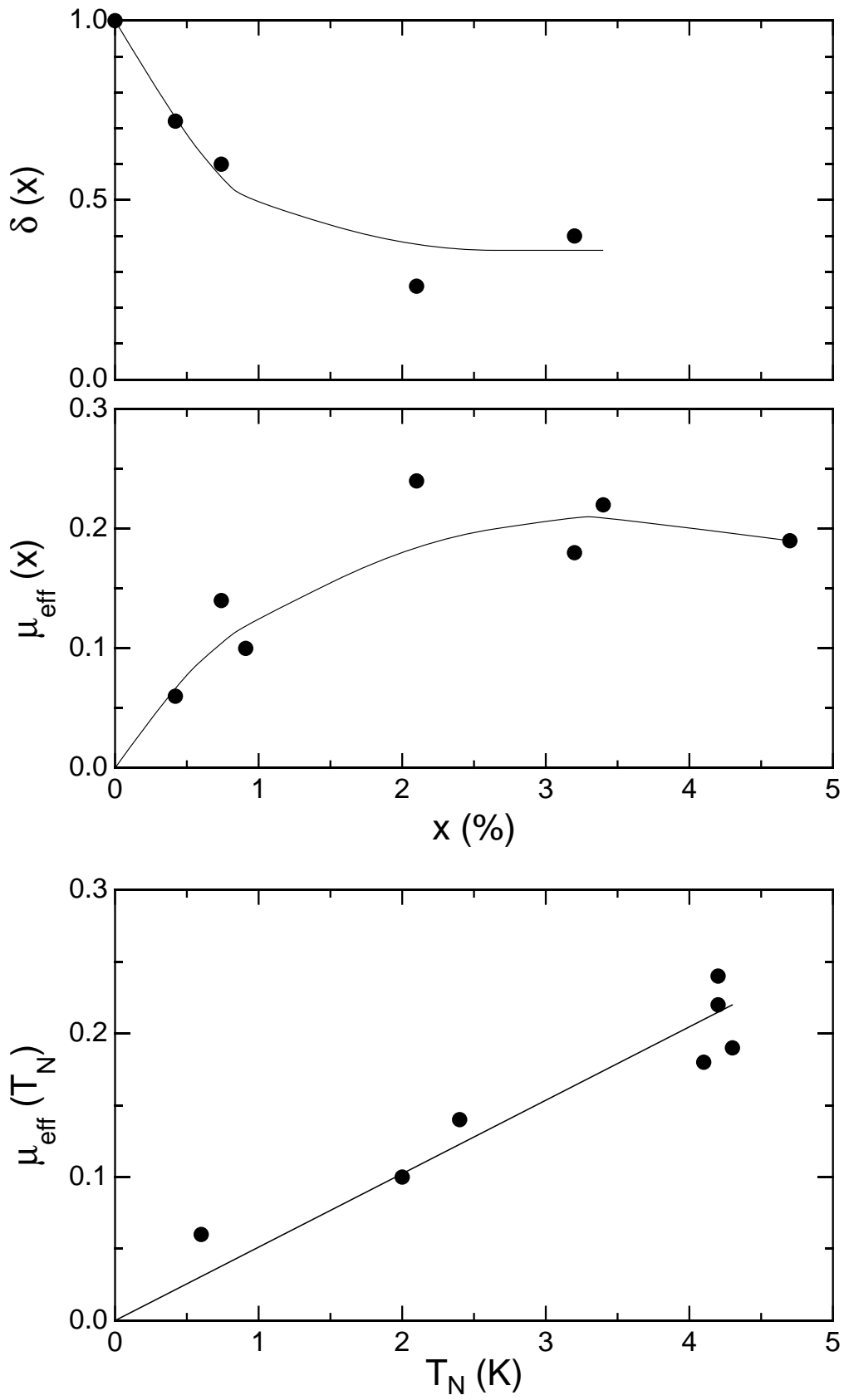
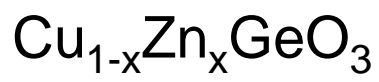




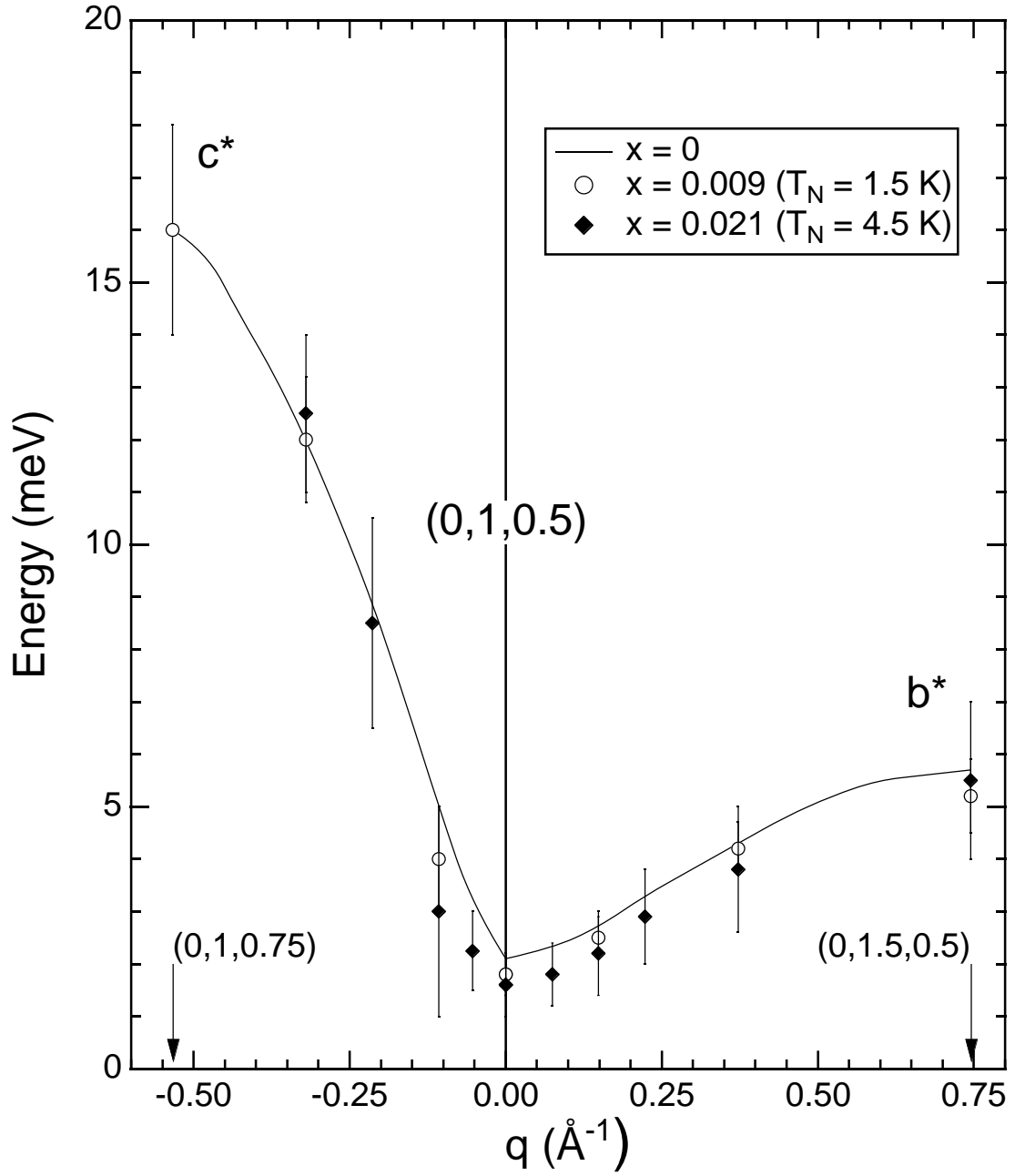
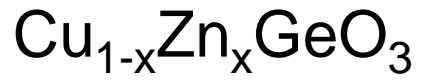
Martin et al., Fig. 3a



Martin et al., Fig. 3b



Martin et al., Fig. 4



Martin et al., Fig. 5

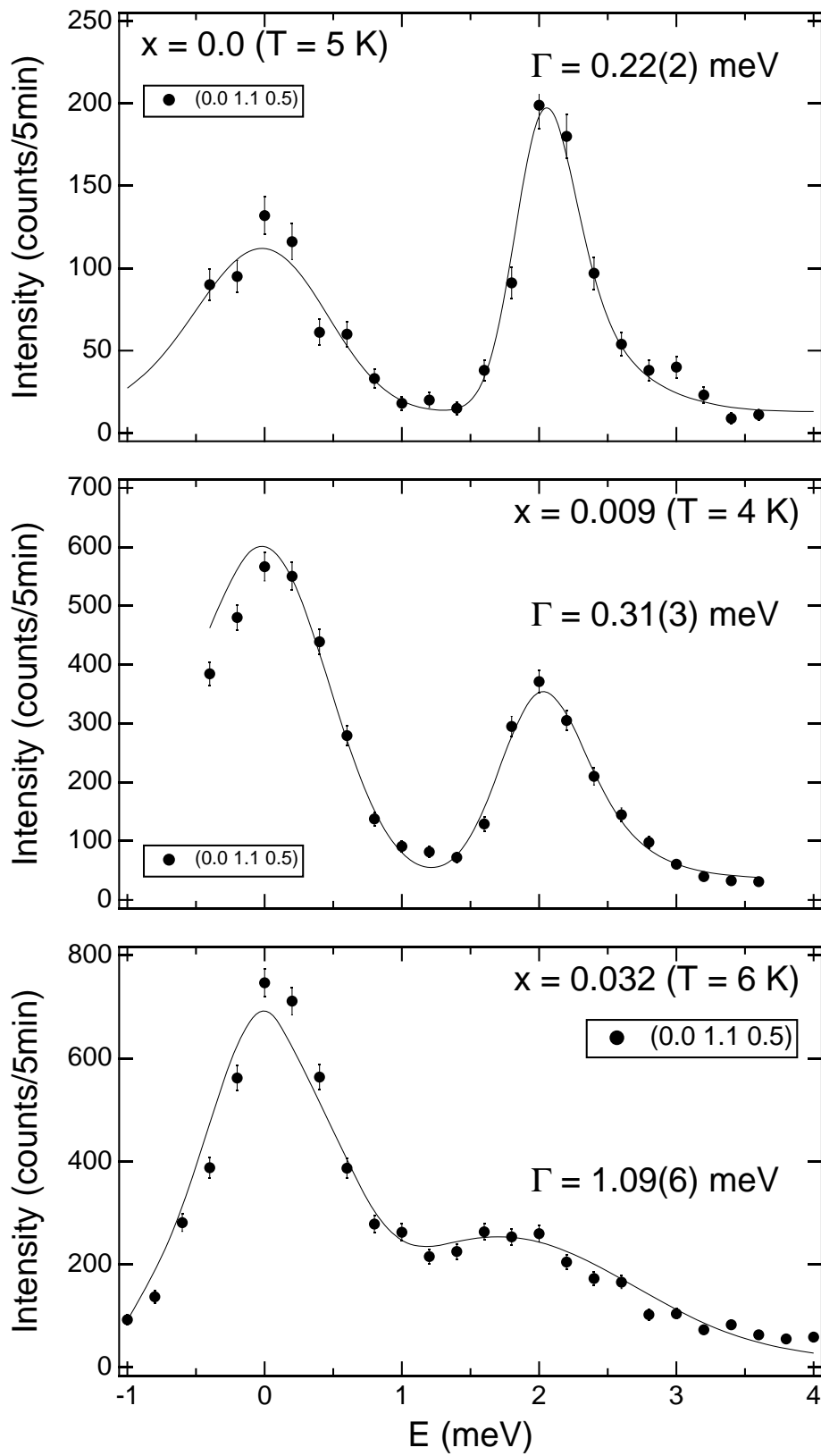
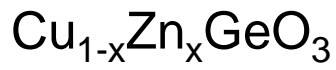


Fig. 6

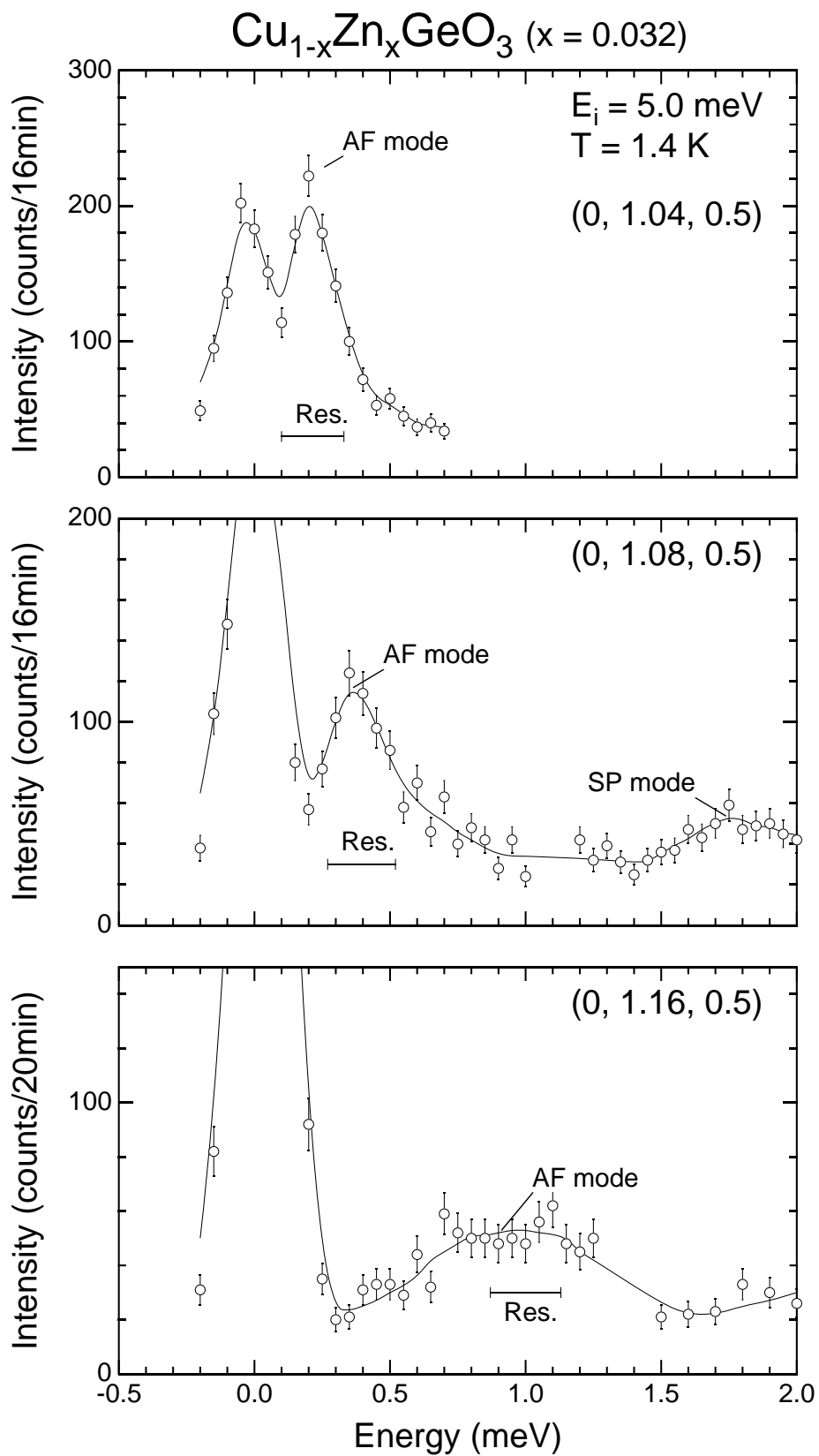
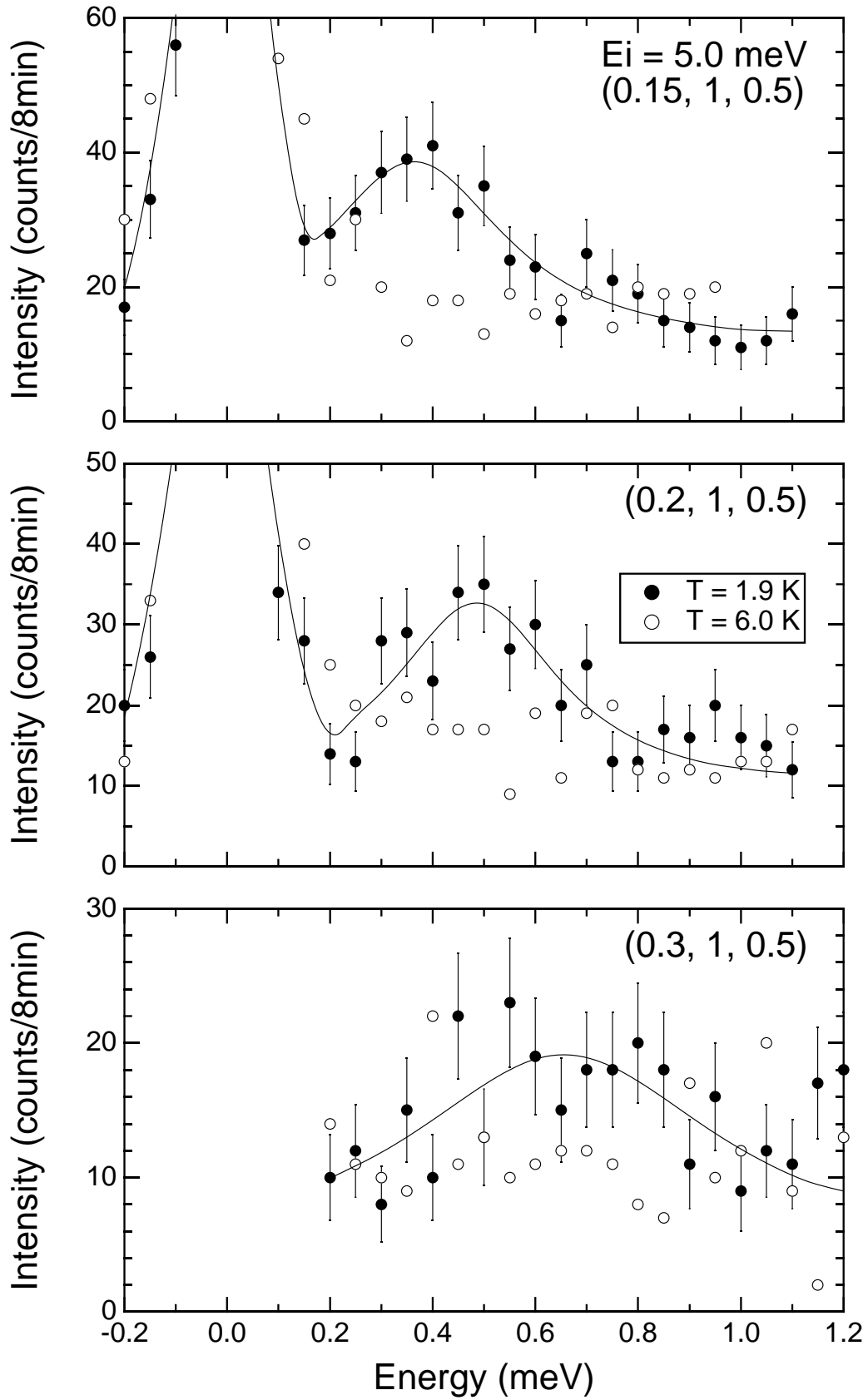


Fig. 7

$\text{Cu}_{1-x}\text{Zn}_x\text{GeO}_3$ ($x = 0.032$)



Martin et al., Fig. 8

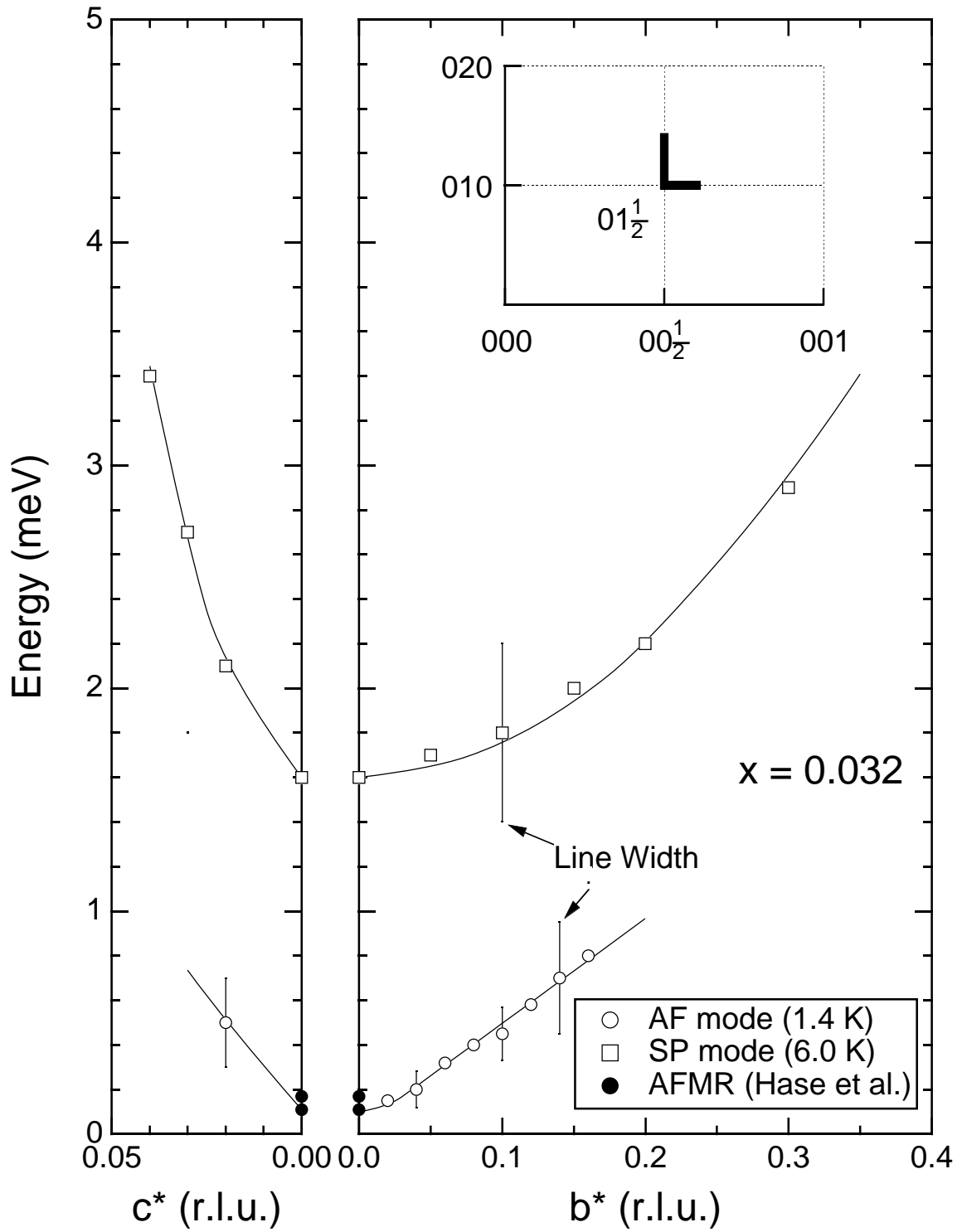
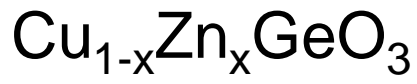


Fig. 9a

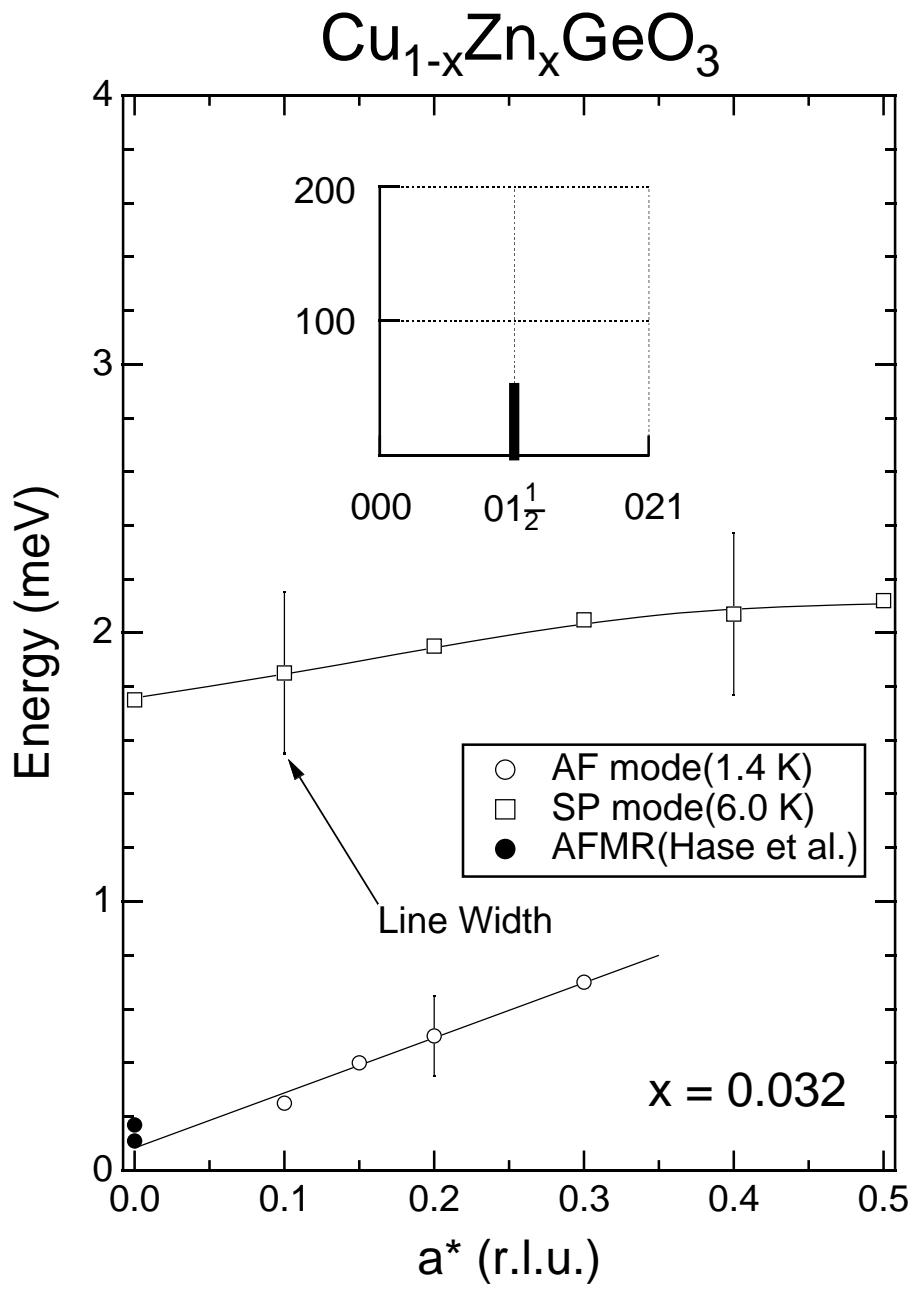


Fig. 9b